Using circular polarization to test the composition and dynamics of astrophysical particle accelerators

Céline Bœhm,[1,2,3,4,*] Céline Degrande,[5] Jakub Scholtz,[2] and Aaron C. Vincent[6,4]

[1]*School of Physics, Physics Road, The University of Sydney, NSW 2006 Camperdown, Sydney, Australia*
[2]*Institute for Particle Physics Phenomenology, Durham University, South Road, Durham, DH1 3LE, United Kingdom*
[3]*LAPTH, U. de Savoie, CNRS, BP 110, 74941 Annecy-Le-Vieux, France*
[4]*Visiting Fellow, Perimeter Institute for Theoretical Physics, Waterloo, Ontario N2L 2Y5, Canada*
[5]*Centre for Cosmology, Particle Physics and Phenomenology (CP3), Université catholique de Louvain, B-1348 Louvain-la-Neuve, Belgium*
[6]*Arthur B. McDonald Canadian Astroparticle Physics Research Institute, Department of Physics, Engineering Physics and Astronomy, Queen's University, Kingston, Ontario K7L 3N6, Canada*

(Received 8 October 2019; revised 30 October 2020; accepted 30 October 2020; published 18 December 2020)

We investigate the production of circularly polarized X and gamma-ray signals in cosmic accelerators such as supernova remnants and active galactic nuclei jets. Proton-proton and proton-photon collisions within these sites produce a charge asymmetry in the distribution of mesons and muons that eventually leads to a net circular polarization signal as these particles decay radiatively. We find that the fraction of circular polarization thus produced is at the level of 5×10^{-4}, regardless of the exact beam spectrum, as long as it is made predominantly of protons. While this fraction is very small, the detection of circular polarization signals in conjunction with high-energy neutrinos would provide an unambiguous signature of the presence of high-energy protons in cosmic accelerators. In supernovae shocks in particular, this would indicate the presence of relativistic protons hitting stationary protons and/or low-energy photons in the intergalactic or interstellar medium.

DOI: 10.1103/PhysRevD.102.123020

I. INTRODUCTION

The observation of cosmic rays (CRs) over several orders of magnitude in energy indicate that particle acceleration occurs in many astrophysical sites and gives rise to high-energy particles which eventually escape and interact with the diffuse surrounding medium. Supernova shocks, massive stars, pulsars, stellar OB associations, and the jets of active galactic nuclei (AGN) are all confirmed sources of cosmic ray acceleration. For a review, see the recent [1].

The maximal cosmic ray energy that can be attained through these processes is not clear yet. However, given their observed gamma-ray spectra, it seems that blazar jets [2] produced by supermassive black holes (SMBHs) at the center of galaxies could be the most powerful accelerators in the Universe, with energies reaching far beyond the PeV scale [3]. The discovery of (extragalactic) PeV neutrinos by the IceCube Neutrino Observatory [4,5] lends further support to the idea that jets associated with SMBHs may be capable of accelerating particles above the PeV scale, although there is still debate on the primary composition of the of particles that are being accelerated (see e.g. [6] and references therein).

Probing the particle content and the dynamics of cosmic accelerators is not an easy task. Here, we argue that the detection of a gamma-ray circular polarization signal from these sites could signal the presence of hadrons and hadronic collisions, independently of an observed neutrino signal. While leptonic processes such as synchrotron radiation also generate a circular polarization depending on the orientation of the magnetic field, the polarization analyzed here is independent of the magnetic field. Our prediction is that hadronic collisions (e.g. proton-proton pp, proton-hadron, and proton-photon $p\gamma$) in cosmic accelerators or in the atmosphere (for a review, see Ref. [7]) produce photons with one dominant polarization state and thus have the potential to create a net right-handed circular polarization signal. Furthermore, this polarization signal is quite frame and energy independent for proton-proton collisions but depends on the kinematics of the initial state for proton-photon collisions. Consequently, the polarization also provides information on the dynamics of the distant accelerators.

This polarization state is uncorrelated with the nature of the magnetic field in these acceleration sites (unlike

*celine.boehm@sydney.edu.au

synchrotron radiation); therefore, the observation of a net circularly polarized γ-ray signal from a cosmic accelerator could reveal the intrinsic nature of its particle content. This conclusion holds whatever the astrophysical site under consideration as long as there is an excess of protons over antiprotons in the initial state. We also note that the interactions of protons in our galaxy and in the atmosphere will give a polarized photon background for new physics searches based on the polarization of x-rays and gamma rays [8,9]. Combined with newly available neutrino data, the observation of a polarized signal would yield further information about the environment in which collisions are taking place, telling us for instance whether pion and muon decays are occurring in an optically thin or thick environment.

There are currently no planned experiments looking for circular polarization of high-energy gamma rays so far, and the detection of such polarization is experimentally challenging. However, we hope that the present results may further encourage development in this direction.

The paper is structured as follows: in Sec. II, we study whether it is possible to generate a circular polarization signal from the decay of Standard Model particles, using analytical arguments. In the same section, we also highlight the relationship between the neutrino flux and the photons produced by these processes [10]. As our analytical study shows that radiative decays could indeed generate circular polarization signal, we compute in Sec. III the fraction of circular polarization expected from the decay of particles produced in proton-proton and photon-proton collisions for various toy configurations, including protons with TeV and PeV energies (and photons with TeV energies, e.g. from a prior CR collision) hitting a stationary target proton or a low-energy photon, as expected when a relativistic jet interacts with the intergalactic medium. We also discuss head-on collisions of protons with center-of-mass energies in excess of the Large Hadron Collider's, as could be expected inside astrophysical acceleration sites. The results for these various toy configurations give us some insights on which parameters are affecting the polarization fraction. Therefore, they help us to understand both the more complicated and realistic case of proton spectrum and which processes can be distinguished thanks to circular polarization. We discuss the results in Sec. IV and conclude in Sec. V.

II. PHOTON AND NEUTRINO SIGNALS

Circular polarization arises from processes where the CP symmetry (the combination of the charge conjugation symmetry C and parity symmetry P) is violated, which generally occurs when the mechanism that produces the gamma ray involves parity-sensitive couplings (i.e. a coupling proportional to the Dirac matrix γ_5) and a charge or particle-antiparticle asymmetry. When these two conditions are met, the photons are produced with one preferred polarization and a net circular polarization signal may be observed from the site of production. We further note that the same electroweak processes which are the source of a net circular polarization signal are also responsible for the generation of high-energy neutrinos. Hence, there is a relationship between the fluxes of unpolarized photons and neutrinos which we will also study in this section.

A. Radiative decay as a circular polarization production mechanism

Hadronic collisions are known to produce hadrons, mesons, leptons, and photons in profusion. The bulk of the photons thus generated originate from strong (non-parity-violating) processes and therefore do not lead to the production of a circular polarization signal. However, a small fraction of the photons produced in these collisions originate from weak, parity-violating processes such as the radiative decay of the neutron (n), charged pion ($\pi^\pm$), kaon ($K^\pm$), and muon ($\mu^\pm$).[1] As proton-proton and proton-photon collisions are expected to produce an excess of n, π^+, K^+, and μ^+ over $\bar{n}, \pi^-, K^-$, and μ^-, all the conditions are met for a circular polarization signal to be generated.[2]

Before investigating whether a charge asymmetry can be generated in hadronic collisions, we start by verifying that such weak decays do generate photons with a preferred polarization state. The main channel to produce photons from muon and meson decays is actually a radiative process.[3] Indeed, although the bulk ($>99\%$) of the charged pions decay into $\pi^\pm \to \mu^\pm \nu_\mu$, a small fraction (about 10^{-4}, though the exact value depends on the IR cutoff imposed on the gamma-ray spectrum) decays radiatively into $\pi^\pm \to \mu^\pm \nu_\mu \gamma$. Similarly, the vast majority of muons decay into $\mu^\pm \to e^\pm \nu_\mu \bar{\nu}_e$, but a small fraction ($\sim 10^{-3}$) decays radiatively into $\mu^\pm \to e^\pm \nu_\mu \bar{\nu}_e \gamma$.

The analytic expressions for these radiative decays were computed in [11] and expressed for both $\mu^\pm$ and $\pi^\pm$ as the ratio of the differential rate to the first-order width[4] Γ_0. We recall these expressions in the next subsection.

1. Pion radiative decay

The polarized pion decay $\pi^\pm \to \ell^\pm \nu_\mu \gamma$, with $\ell^\pm = \mu^\pm$ or $e^\pm$ takes the form [11]

[1]We will neglect the contribution from the τ leptons as they are not abundantly produced in the processes considered here.

[2]There are other P-violating weak subprocesses of the hadronic collision whose radiative corrections could lead to net photon polarization; however, there are subleading by many orders of magnitude.

[3]We will not discuss in this section the decays of the neutron and kaon, but they follow the same pattern as described below.

[4]For the process $\pi^+ \to e^+ \nu \gamma$, Γ_0 would correspond to $\pi^+ \to e^+ \nu$ and not the full decay rate of the pion.

$$\frac{1}{\Gamma_0}\frac{d\Gamma^{(\lambda_\ell,\lambda_\gamma)}}{dxdy} = \frac{\alpha}{2\pi}\frac{1}{(1-r_\ell)^2}\rho^{(\lambda_\gamma,\lambda_\ell)}(x,y), \tag{1}$$

with

$$\rho^{(\lambda_\gamma=\pm1,\lambda_\ell)}(x,y) = f_{IB}^{(\lambda_\gamma,\lambda_\ell)}(x,y) + \frac{m_\pi^2}{f_\pi^2}\frac{(V\pm A)^2}{4r_\ell}f_{SD}^{(\lambda_\gamma,\lambda_\ell)}(x,y) + \frac{m_\pi}{f_\pi}\frac{(V\pm A)^2}{4r_\mu}f_{INT}^{(\lambda_\gamma,\lambda_\ell)}(x,y). \tag{2}$$

In these expressions, $x = 2E_\gamma/m_\pi$, $y = 2E_e/m_\pi$, $r_\ell \equiv m_\ell^2/m_\pi^2$, and $\lambda_\gamma, \lambda_\ell$ are the polarization of the photon and lepton, respectively, ($L = -1$ and $R = +1$) and V (A) is the vector (axial) form factor of the pion, which we take from [12]. In what follows, we will use $f_\pi = 0.131$ GeV. Three processes contribute to this expression, namely, (i) internal bremsstrahlung emission (IB) from either the initial or final state charged particle, (ii) "structure-dependent" emission (SD) from the intermediate hadronic state, and (iii) an interference term (INT) between the two former contributions. Their analytic forms are given in Appendix A of Ref. [11].

2. Muon radiative decay

The radiative decay of the muon $\mu^\pm \to e^\pm\nu_\mu\nu_e\gamma$ has the following form:

$$\frac{1}{\Gamma_0}\frac{d\Gamma^{(\lambda_e,\lambda_\gamma)}}{dxdy} = \frac{\alpha}{24\pi}\frac{1}{A_e x}(G_0 + \lambda_\gamma\bar{G}_0 + \lambda_e(G_1 + \lambda_\gamma\bar{G}_1)), \tag{3}$$

where λ_e and λ_γ are, respectively, the electron and photon polarizations, $x = 2E_\gamma/m_\mu$, $y = 2E_e/m_\mu$, and $A_e = \sqrt{y^2 - 4m_e^2/m_\mu^2}$. $G_{0,1}$ and $\bar{G}_{0,1}$ are polynomials in x and y which can be found in Appendix B of [11].

B. Photon spectra

The above expressions were given for pion and muon decaying at rest. However, the mesons and leptons produced by hadronic collisions are not at rest, so photons must be successively boosted from the muon frame to the pion frame (if relevant), and subsequently to the "lab" frame of the observer.

The spectrum from the two-stage process $\pi \to \mu\nu$, $\mu \to e^-\nu_e\nu_\mu\gamma$ is given by

$$\frac{d\phi_\gamma}{dE_\gamma} \sim \int d\Omega dE_{CM}\Lambda(E_{\gamma,\mathrm{lab}}, E_{\gamma,CM})\frac{d\Gamma}{dE_{\gamma,CM}}\frac{d\phi_\pi}{dE_\pi}, \tag{4}$$

where Λ represents the boosts and rotations from the pion frame to the lab frame, and $d\phi_\pi/dE_\pi$ is the pion spectral distribution in the lab frame. Equation (4) can equally be adapted to the muon decay spectrum, and sequential decays can be seen as nested integrals of the same form.

To explicitly evaluate the spectrum in the observer's frame, it is more practical to construct a simple Monte Carlo simulation, which treats the differential decay rates as a probability distribution function (PDF). We first draw a photon with a random orientation, with an energy taken from the distribution given by (2) or (3). This photon is then boosted to the lab frame and, by repeating the procedure for many photons, one eventually obtains the spectrum as seen by the observer.

In the case of the two-step muon photons, the photon must first be boosted to the parent pion's frame, then boosted again to the lab frame, keeping track of the random direction of motion of the intermediate muon. We have verified that our results agree with the output of the effective models implemented in MadGraph5_aMC@NLO. The advantage of this approach being faster sample generation and somewhat more transparent physics, thanks to the analytic form. We give the details of our prescription in the Appendix.

Note that if we want the full spectrum down to $y = 2E_\gamma/m$, there is some subtlety: the cross section at leading order is IR divergent. This divergence is canceled by the one-loop corrections to the polarized (non-bremsstrahlung) cross section. This is normally circumvented by including a cut in $E_{\gamma,min}$, corresponding to the minimum photon energy seen by the detector. We place this cutoff at $E_{min,\gamma} = 10$ MeV in the pion rest frame.

We present the flux of circularly polarized photons expected from pion and muon decays in Fig. 1, assuming a pion energy spectrum given by

$$\frac{d\phi_\pi}{dE_\pi} \propto E^{-\alpha}. \tag{5}$$

For concreteness, we choose $\alpha = 2.3$, which coincides approximately with the expected pion spectrum from proton-proton collisions (see Sec. III).

The contribution to the radiative photon flux from the pion decay (2) into muons and electrons is shown in red and purple, respectively. The radiated photon from muons is shown in blue. The total (black) overlaps with the blue line due to the overwhelmingly dominant contribution from muon decay. The dashed lines represent the right-handed (positive) polarized flux, while solid lines are left-handed (negative).

The high-energy slope of the spectrum is determined by the spectral index of the pion flux, whereas the location of the break between the plateau and the slope is due to the minimum injected pion energy (135 GeV in this case). The bottom panel of Fig. 1 shows the fractional polarization of our signal. Above 50 GeV, about 80% of the photons radiated from a positive pion have a right-handed

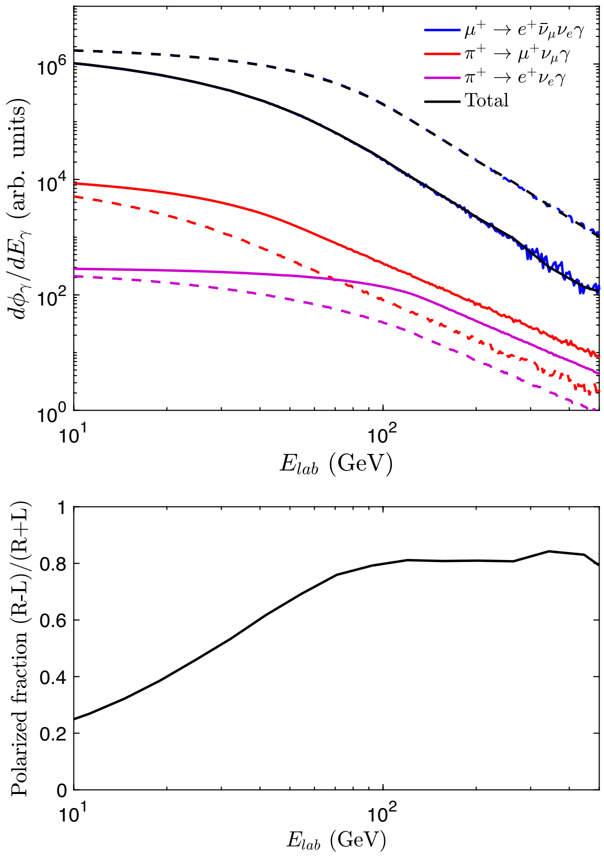

FIG. 1. Polarized photons produced from the decay of a distribution of π^+, with a power law distribution in energies $d\phi_\pi/dE_\pi \propto E^{-\alpha}$, with $\alpha = 2.3$, and lower energy $E_{\rm min} = 135$ GeV. Photon polarizations are represented by solid (left-handed) and dashed (right-handed) lines. Top: contributions to the total polarized flux; bottom: fractional contribution to the total flux of photons from charged pion decay from left- ($P = -1$) and right-handed ($P = +1$) circularly polarized photons.

polarization. Negative pion (π^-) decay would result in the exchange of L and R polarized photons.

Figure 1 shows that as long as there is some asymmetry between π^+ and π^- production rates, there will be a net circular polarization in CR acceleration sites.

C. High-energy neutrino signature

In the previous subsection, we argued that a net charge asymmetry in the initial state together with parity-violating interactions is at the origin of the final photon polarization. Here we briefly turn our attention toward neutrinos. The relationship between neutrino flux and total gamma-ray emission is well known (see e.g. [13–15]): gamma production in CR collisions dominantly comes from neutral pions, and the relationship between neutral and charged pion production guarantees such a correlation. Here, we show that this also leads to a relationship between the flux of neutrinos and the fluxes of *polarized* photons.

The origin of this relationship stems in the fact that isospin is a good symmetry in a high-energy pp and $p\gamma$ interactions. That is, charged and neutral pions are expected to be produced equally frequently. Since neutral pions are the dominant source of unpolarized photons and charged pions are the dominant source of neutrinos, one expects the unpolarized photon and neutrino fluxes to be related, as discussed. To demonstrate this explicitly, we consider the decay of a pion at rest into a final state that contains a particle i and call $f_i(\mathcal{E})$ the distribution function (which is related to the flux $d\phi_i/dE_i$) in terms of quantity $\mathcal{E} = E + p_z$ in the rest frame of the decaying pion. In the lab frame, boosted by γ, the energy of this particle is

$$E_{\rm lab} = \gamma(E + \beta p_z) \sim \gamma(E + p_z) = \gamma\mathcal{E}. \qquad (6)$$

The above expression assumes $\beta \sim 1$ because we are interested in highly boosted neutrinos that we can see in IceCube and other similar neutrino detectors.

Denoting $g_{\pi^0}(\gamma)$ the distribution function of the boosts of the neutral pions, Eq. (4) can be simplified in terms of the boosts (γ) and $\mathcal{E}$ so that the distribution functions for the energies of particles i in the lab frame [i.e. the differential flux [expected to be measured by the observer)] read

$$h_i(E_{\rm lab}) = \int d\gamma d\mathcal{E}\delta(E_{\rm lab} - \gamma\mathcal{E}) g_{\pi^0}(\gamma) f_i(\mathcal{E}). \qquad (7)$$

The distribution functions $f_i(\mathcal{E})$ can be evaluated analytically or using Monte Carlo methods as in the previous section. In the case $\pi^0 \to \gamma\gamma$, f_γ is particularly simple,

$$f_\gamma(\mathcal{E}) = \begin{cases} \frac{2}{m_{\pi^0}} & 0 < \mathcal{E} < m_{\pi^0}, \\ 0 & \text{otherwise.} \end{cases} \qquad (8)$$

The normalization of the above distribution is equal to 2, because there are two photons per neutral pion. As a result, the h_γ from Eq (7) can be evaluated analytically using

$$h_\gamma(E_{\rm lab}) = \frac{2}{m_{\pi^0}} \int_{E_{\rm lab}/m_{\pi^0}}^{\infty} \frac{d\gamma}{\gamma} g_{\pi^0}(\gamma). \qquad (9)$$

The fundamental theorem of calculus then guarantees that

$$g_{\pi^0}(\gamma) = -\gamma \frac{m_{\pi^0}^2}{2} \frac{dh_\gamma}{dE_{\rm lab}}\bigg|_{E_{\rm lab} = \gamma m_\pi}. \qquad (10)$$

The boost distribution $g_{\pi^0}(\gamma)$ for the neutral pions can then be derived using Eq. (10) from the measured photon spectrum (h_γ assuming that all the photons come from the decay of neutral pions). Once $g_{\pi^0}(\gamma)$ is known, one can easily compute the expected neutrino spectra using Eq. (7) and assuming $g_{\pi^+} = g_{\pi^-} = g_{\pi^0}$.

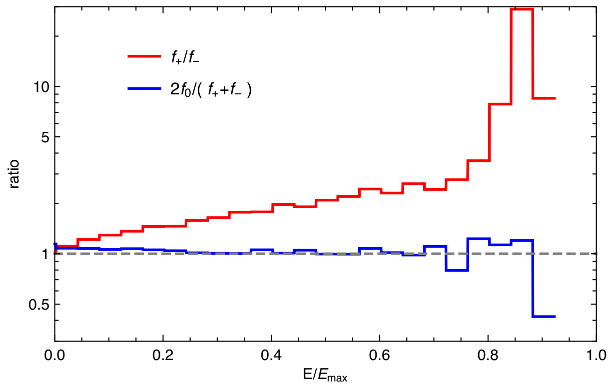

FIG. 2. Ratios of pion energy distribution functions for 500 TeV protons impinging on protons at rest. Note that while the charge asymmetry grows steadily for larger energies, the neutral to charged pion flux stays much more stable.

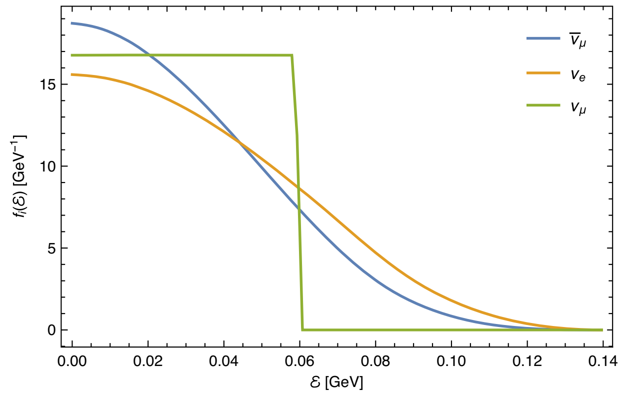

FIG. 3. Distributions $f_i(\mathcal{E})$, where $\mathcal{E} = E + p_z$, for different decay products of π^+ in the decay channel $\pi^+ \to \mu^+\nu_\mu \to e^+\nu_\mu\bar{\nu}_\mu\nu_e$. The distributions for decays of π^- can be obtained by charge conjugation.

The results are shown in Fig. 4 (top panel) where we display the ratio of the neutrino flux obtained directly from PYTHIA to the neutrino flux derived from the PYTHIA photon flux. As one can see, the agreement is excellent and so we can be confident in our simulations.[5] We note that the photon flux extends to higher energies than the neutrino flux. This is expected since neutral pion decays into two photons, while the charged pion eventually produces four stable particles, reducing the available energy per neutrino. The kinematics associated with these two processes being different, the photon flux cannot be used to predict the neutrino flux up to the same energy; hence, the mismatch between the cutoff locations is in Fig. 4.

The accuracy of the relationship $g_{\pi^+} + g_{\pi^-} \simeq 2g_{\pi^0}$ can be seen from the blue line in Fig. 2, which shows the ratios of pion distributions resulting from pp collisions at 500 TeV. This ensures a relationship between the photon and neutrino fluxes.

Conversely, the fact that $g_{\pi^+} \neq g_{\pi^-}$ (red line in Fig. 2) leads to our net polarization signal as well as a neutrino-antineutrino asymmetry. This is detectable in principle, since the ν-nucleon and $\bar{\nu}$-nucleon cross sections differ by a small amount. However, astrophysical and detector uncertainties make this extremely difficult. The difference could be noticeable in the case of electron neutrinos thanks to the Glashow resonance at $E_{\bar{\nu}_e} = 6.3$ PeV.

III. NET CIRCULAR POLARIZATION

Our analytical calculations have already indicated that the radiative decays of pions and muons should generate photons with a preferred polarization state if there is a charge asymmetry in the initial state. We now show that both inclusive pp and $p\gamma$ collisions can generate the required charge asymmetry (i.e. an excess of μ^+ over μ^- etc.) to eventually lead to a net circular polarization signal in cosmic accelerators.

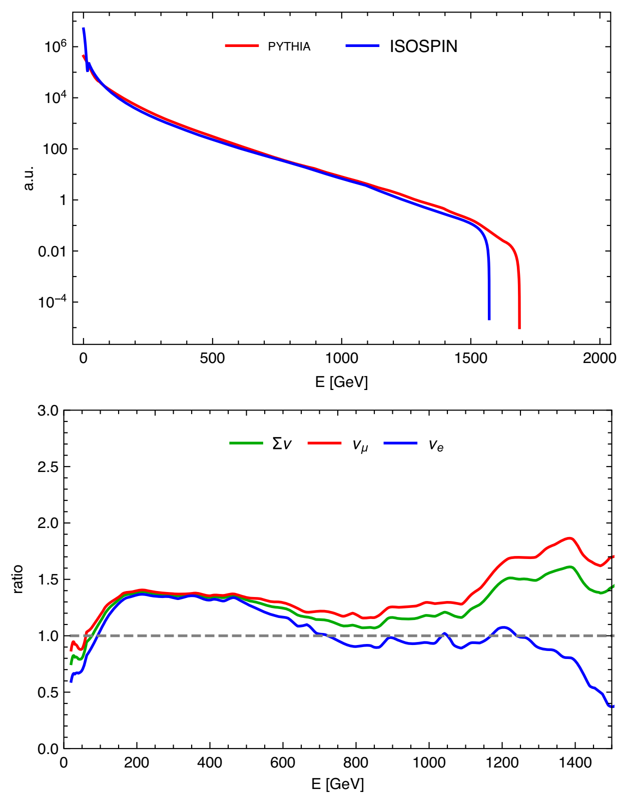

FIG. 4. The top figure shows the comparison between the neutrino spectrum computed by PYTHIA and the neutrino flux predicted from the photon flux using the method of Sec. II C from pp collisions at 2 TeV. The bottom figure shows the ratios for different neutrino species (where the sum over neutrino and antineutrino species is implied). Note that the isospin method is not reliable at high energy.

[5] We have calculated the functions f_{ν_j} by numerically integrating over the full matrix element for the decay and shown them in Fig. 3.

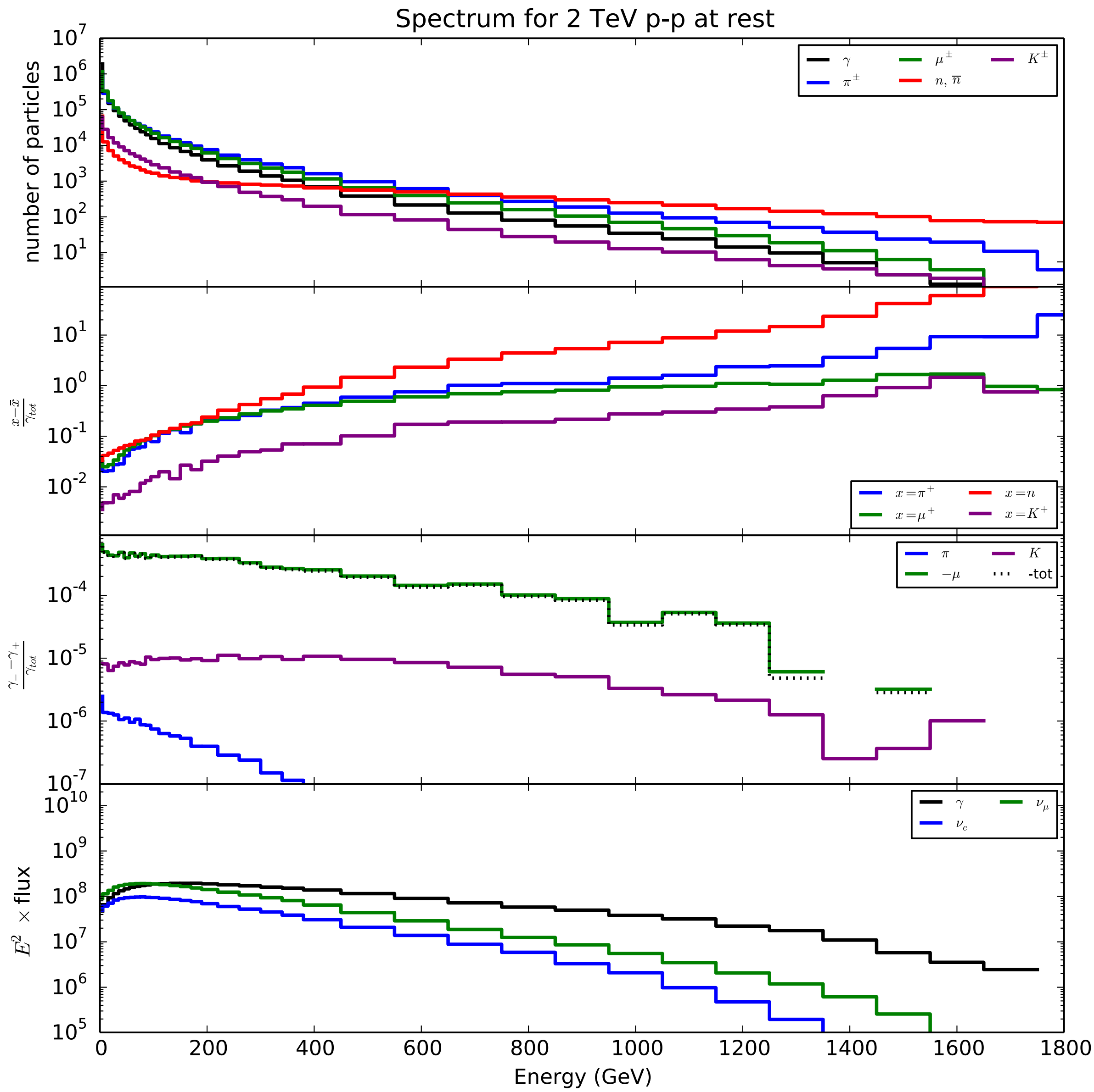

FIG. 5. Photon, charged pion, charged kaon, neutron, muon, and neutrino spectra for 2 TeV protons hitting protons at rest, based on 200,000 events. The first panel shows the total spectrum of the particles from PYTHIA but also from the charged pions and kaons decays for the pions and muons and the photons of each polarization from the charged pion, charged kaon, neutron and muon decays. The only cut on the photon is on its energy: $E_\gamma > 0.01$ GeV. The second panel displays the particle/antiparticle asymmetry relative to the photon spectrum. The polarization fraction is shown on the third panel. In the muon case, the plotted quantity is $\gamma_+ - \gamma_-$ since μ^+ produces dominantly right-handed photons. The neutrino spectrum is displayed in the last panel.

A. Schematic procedure

We use the PYTHIA8 software [16–18] to simulate the nature and energy of the particles produced by the pp and $p\gamma$ collisions. The photon spectra on which we base our conclusions are obtained in a three-step procedure summarized below.

(1) All the products of the collisions—except for neutrons, charged pions, charged kaons, and muons—are allowed to decay. This is achieved by artificially setting the distance parameter in PYTHIA (which in the LHC context represents the distance between the "detector" and the collision) to 10^{18} mm,[6] since the observation is expected to happen very far from the interaction point in astrophysics, contrary to colliders. This parameter should also be changed if interactions of CR in the atmosphere are considered instead.

[6]For consistency, we checked that the photons thus obtained were produced by parity conserving processes.

(2) The neutron, charged pion, and muon decays are computed using the MadGraph5_aMC@NLO [19,20]. The pions and muons produced by the decay of the kaons are then added to their respective spectra.
(3) Finally, we simulate the pion and muon decays using MadGraph5_aMC@NLO to obtain the polarized photon spectra.

We do not keep the spin information from the first two steps. This could slightly affect our estimates of the polarization fraction, but this is not expected to have a major impact on the final results. In addition, PYTHIA8 has not been calibrated beyond a few TeVs yet (in the center-of-mass energy). Therefore, the normalization of the hadronic spectra may not be exact at very high energy. In practice, this corresponds to cosmic ray energies above a few tens of PeV. Finally, we mention that the center-of-mass energies in all the considered cases are well above the resonances of the $p-p$ and $p-\gamma$ cross-sections, as PYTHIA does not include such processes. These do not contribute to the $p-p$ collisions at these energies; for $p-\gamma$ collisions, we do note that resonances could increase the production of charged pions.

B. Setup

We use the same parametrization of PYTHIA8 as the ATLAS Collaboration [21] in their recent measurement of the inelastic pp cross section. That is, we use the Monash [22] set of tuned parameters with the NNPDF 2.3 LO PDF and the pomeron flux model of Donnachie and

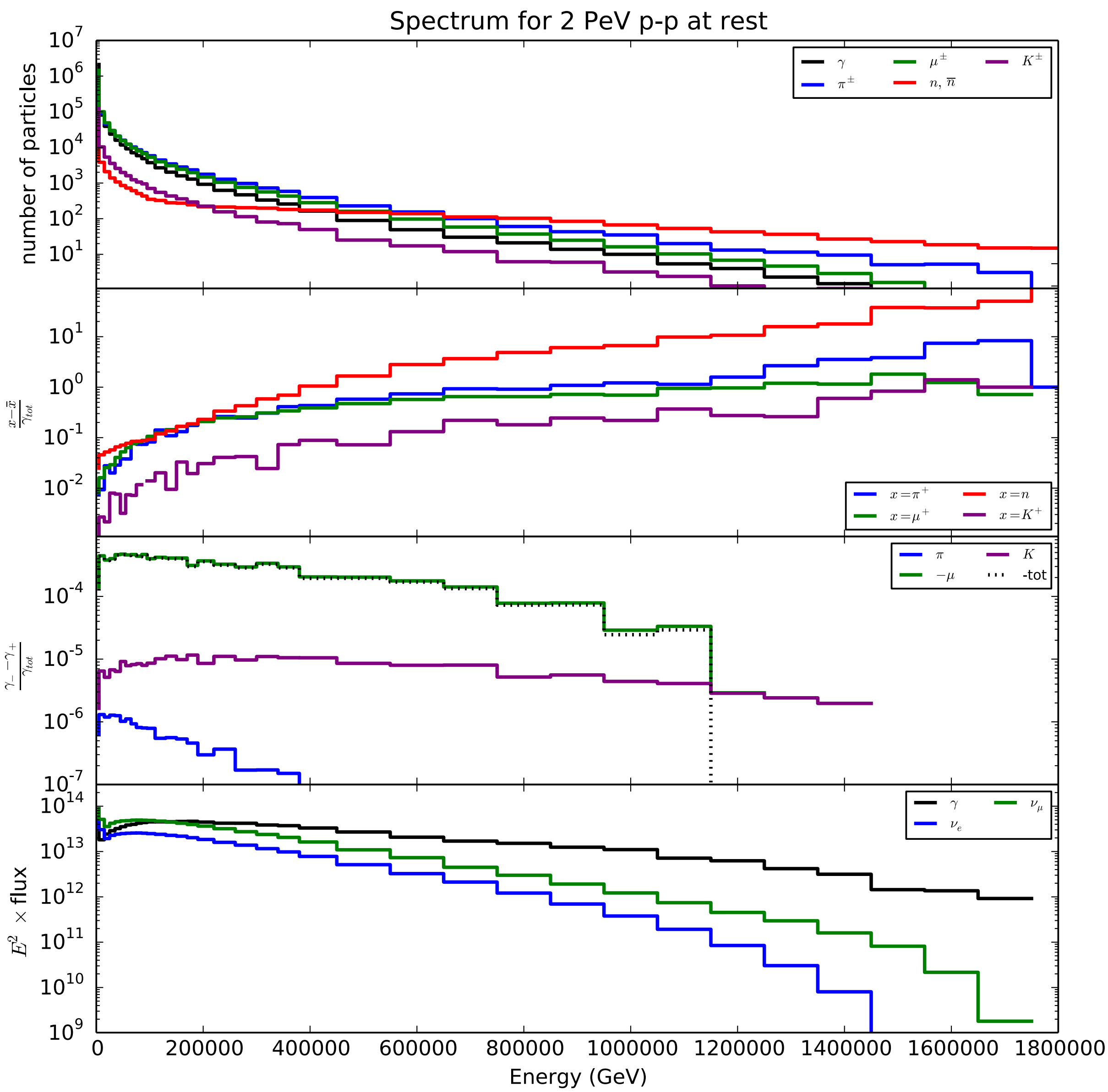

FIG. 6. Same as Fig. 5 for 2 PeV protons hitting protons at rest. We have not included the effects of propagation which lead to attenuation and appearance of an energy cutoff.

Landshof [23]. The parameters describing the pomeron Regge trajectory are set to $\alpha' = 0.25$ and $\epsilon = 0.1$. This configuration gives an inelastic cross section of 78.4 mb at 13 TeV consistently with the ATLAS measurement.

The output from PYTHIA (step 1) only contains stable particles (photons, electrons, protons, neutrinos) plus the neutrons, charged pions, kaons, and muons for which the decay has been switched off. The spectra for these four sets of particles (neutrons, charged pions, kaons, and muons) are displayed in Figs. 5 and 6 as solid lines for four scenarios: (i) a collision of a 2 TeV proton on a proton at rest, (ii) a collision of a 2 PeV proton on a proton at rest, (iii) a collision of two 6.5 TeV protons in the center-of-mass frame, and (iv) a collision of two 500 TeV protons in the center-of-mass frame. The latter two scenarios are not expected to play a role in astrophysics. However, they serve to illustrate how frame and energy independent our result is.

The photons produced in the PYTHIA's output are unpolarized since they come from the decay of mesons into two photons or the decay of excited QCD states into lower QCD states without changing the flavor of the constituent quarks and neither processes can induce polarized photons (the initial state of the former is parity-even and the latter is dominated by the strong and electromagnetic interactions, which conserve parity).

The pion decay is induced by the coupling of the W boson to the leading term of the left-handed current of the chiral perturbation Lagrangian,

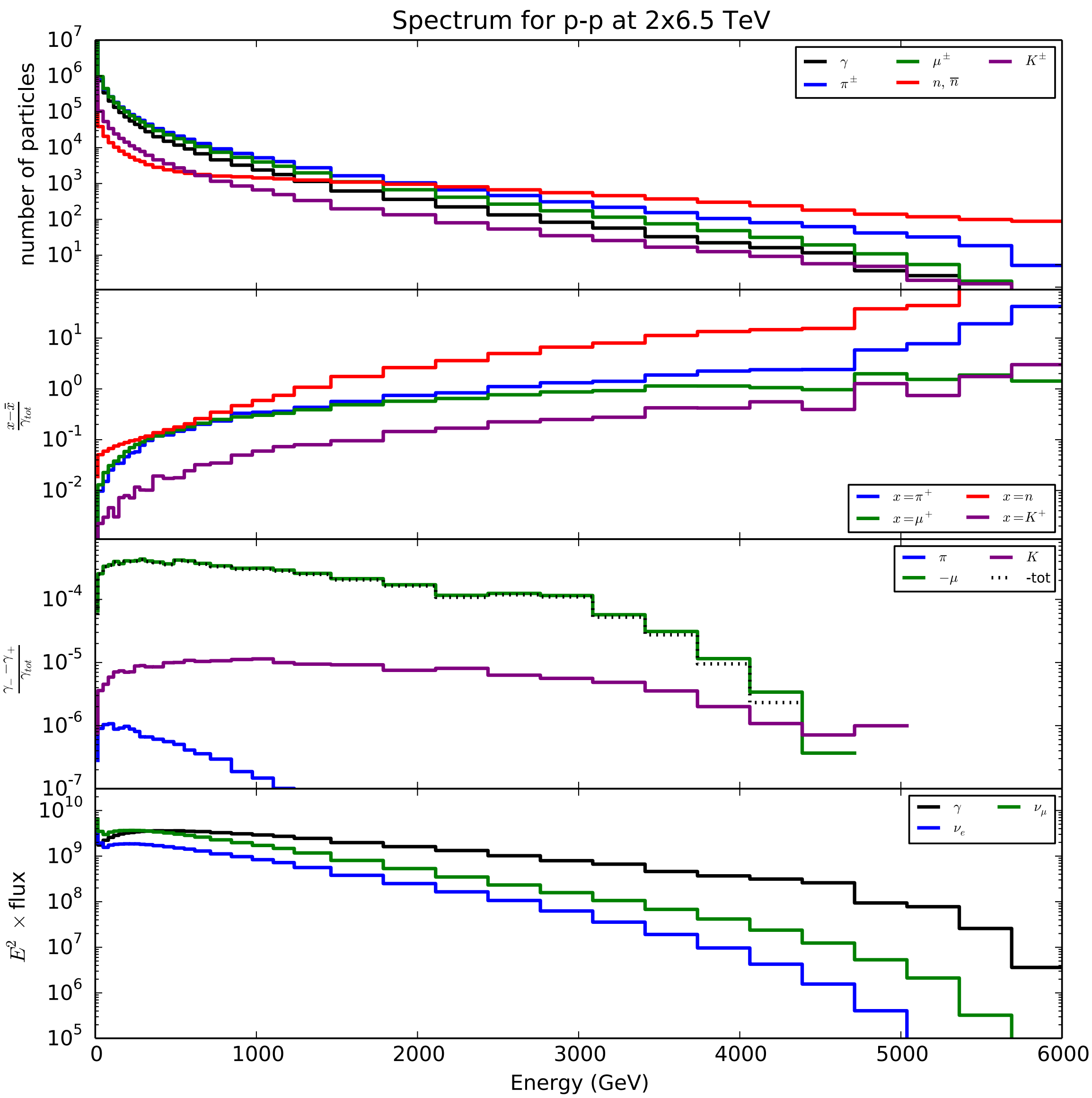

FIG. 7. Same as Fig. 5 for proton collision at 13 TeV, in the center-of-mass (CM) frame. We have not included the effects of propagation which lead to attenuation and appearance of an energy cutoff.

$$\frac{g_w f_\pi}{2\sqrt{2}} V_{ud} \partial_\mu \pi^- W^\mu, \tag{11}$$

where g_w is the weak coupling constant, f_π is the pion decay constant, and V_{ud} is the Cabibbo-Kobayashi-Maskawa matrix element. The neutron decay is induced by the following interaction:

$$g_n \bar{p} \gamma^\mu (1 + r_{AV} \gamma_5) n W_\mu, \tag{12}$$

where the overall coupling g_n is fixed to give the measured total decay width of the neutron and the ratio of the axial and vector couplings is fixed at its particle data group value $r_{AV} = -1.2723$ [12].

The decay of the neutrons, charged pions, kaons, and muons are computed in a second step using MadGraph5_aMC@NLO and the low-energy models [including the effective interactions Eqs. (11) and (12)] implemented in FeynRules [24,25]. We start with the kaon decay as they produce more muons and pions through $K^+ \to \mu^+ \nu_\mu$, $K^+ \to \pi^0 \pi^+$, and $K^+ \to \gamma \mu^+ \nu_\mu$ (and charge-conjugate processes). We do not need to include the radiative corrections to K decays into pions. These branching ratios are small and no net photon polarization can be induced in these processes. The resulting charged pions and muons are added to the spectra obtained from PYTHIA and later decayed into $\pi^+ \to \mu^+ \nu_\mu$, $\pi^+ \to \gamma \mu^+ \nu_\mu$, $\mu^+ \to e^+ \nu_\mu \bar{\nu}_e$, and $\mu^+ \to \gamma e^+ \nu_\mu \bar{\nu}_e$, respectively. The photons from the decay of the neutral pions are added to the unpolarized photon spectrum obtained in step 1. We have not included the

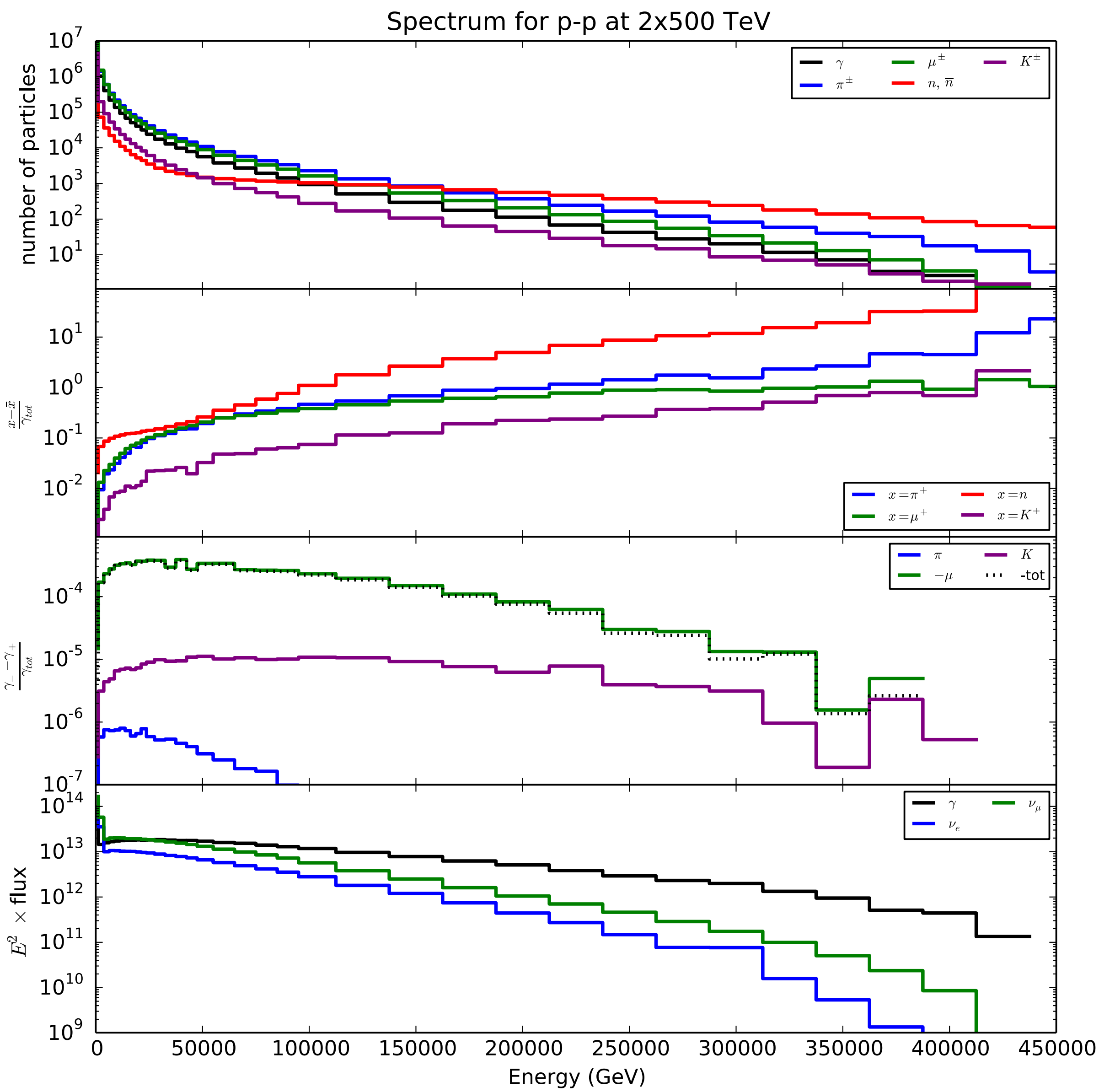

FIG. 8. Same as Fig. 5 for proton collision at 1 PeV, in the center-of-mass (CM) frame. We have not included the effects of propagation which lead to attenuation and appearance of an energy cutoff.

neutrinos produced by the neutron decays ($n \to pe^-\nu$ and $n \to pe^-\nu\gamma$) to the initial neutrino spectrum produced by PYTHIA as these decays are very strongly phase-space suppressed.

Note that the convolution between the events from PYTHIA and the decay by MadGraph5_aMC@NLO is not done event-by-event but bin-by-bin using the bin center as the initial energy of every particle within each bin. We have checked however that a reduction of the binning by a factor 2 gives the same result within the numerical accuracy resulting from the limited number of events.

C. Polarization fraction from inclusive *pp* collisions

The net circular polarization signal that is generated from pp collisions is displayed in the third panel of Figs. 5–8. All four cases display a very similar behavior, i.e. a polarization fraction on the order of 10^{-3} that decreases very slowly with energy. The nonzero polarization is due to the combination of an asymmetry between particles and antiparticles (as seen in the second panel), and the degree to which parity is violated in the decay processes.

While neutrons produce the largest circular polarization signal, all the photons that they produce have a very low energy due to the small phase space of the decay. They therefore end up in the lowest energy bin. This explains why the dominant contribution to the polarization fraction is from the muon decays.

Since the protons in a typical CR acceleration site are not monoenergetic but have a continuous energy distribution, we display in Fig. 9 the result for collisions between

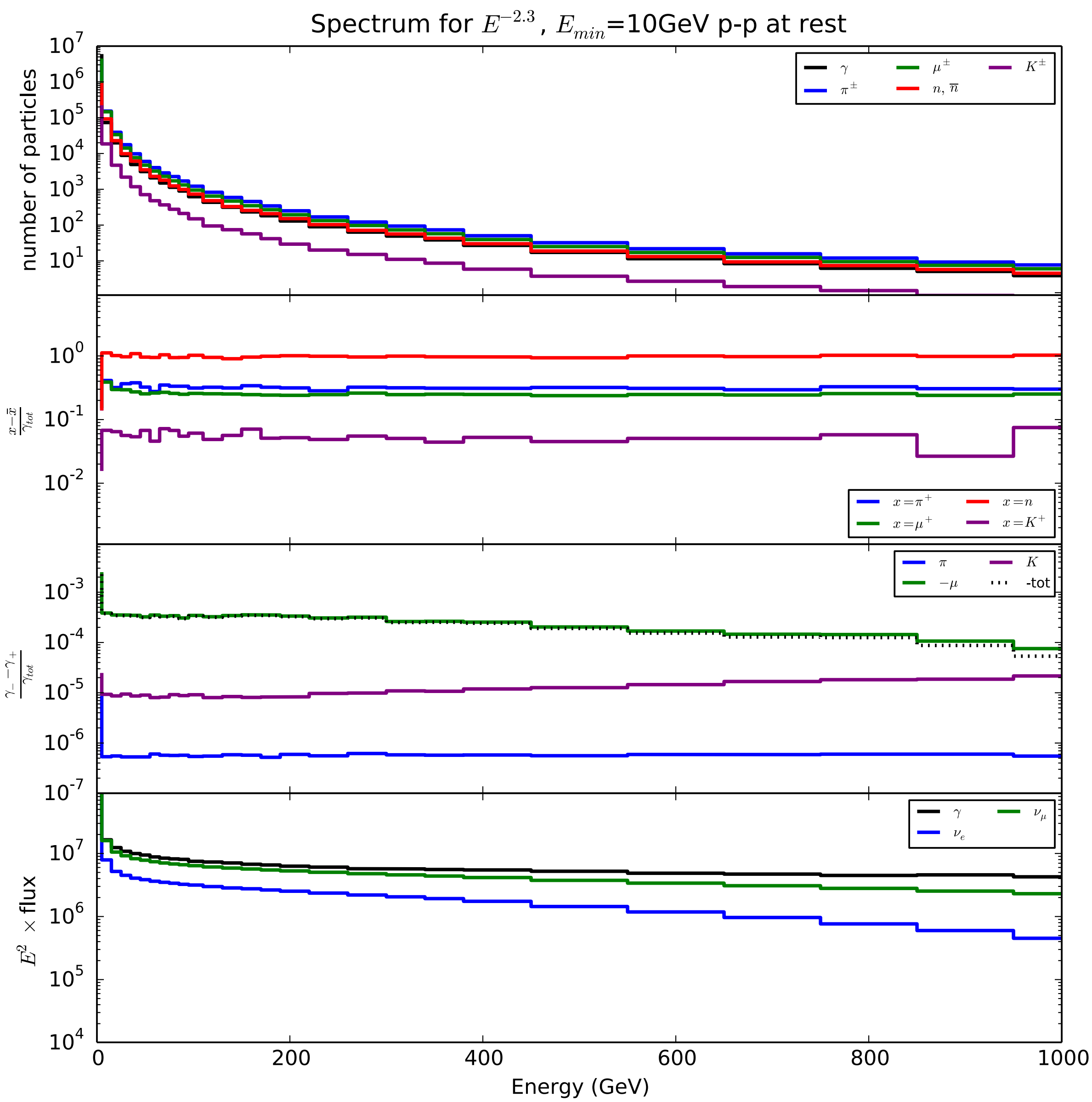

FIG. 9. Same as Fig. 5 but for protons with a power law spectrum $E^{-2.3}$ with a minimum energy of 10 GeV hitting protons at rest.

protons at rest and a beam of protons with a power law spectrum, i.e. $\propto E^{-2.3}$ [26], with the minimal energy of the proton set at 10 GeV. The polarization fraction is quite similar to the fixed energy case since it does not vary much with the initial energy of the protons or with the photon energies. Given this similarity, we anticipate that changing the spectral index will have little effect on our conclusions.

Although the results of PYTHIA have been heavily compared to experimental data, the initial asymmetry in the pion and muon sector from pp interactions has not been experimentally confirmed yet. A few measurements have been made by CMS to compare the charged hadron and antihadron production [27]. However, the precision is insufficient to confirm this effect. In addition, the CMS experiment focuses on low-energy hadrons which contribute very little to the photon polarization. Therefore, our result should be seen as the best prediction that can be made so far.

D. Polarization fraction from inclusive $p\gamma$

Proton-photon collisions are also simulated with PYTHIA8, using the default setting which gives a total cross section in agreement with H1 [28]. The procedure to obtain the photon polarization is identical to the one used for proton-proton collisions. The results for collisions of 2 TeV photons on protons at rest are shown in Fig. 10. Since SNRs such as the Crab are known to be high-energy gamma-ray sources that extend beyond 100 TeV [29,30], this could

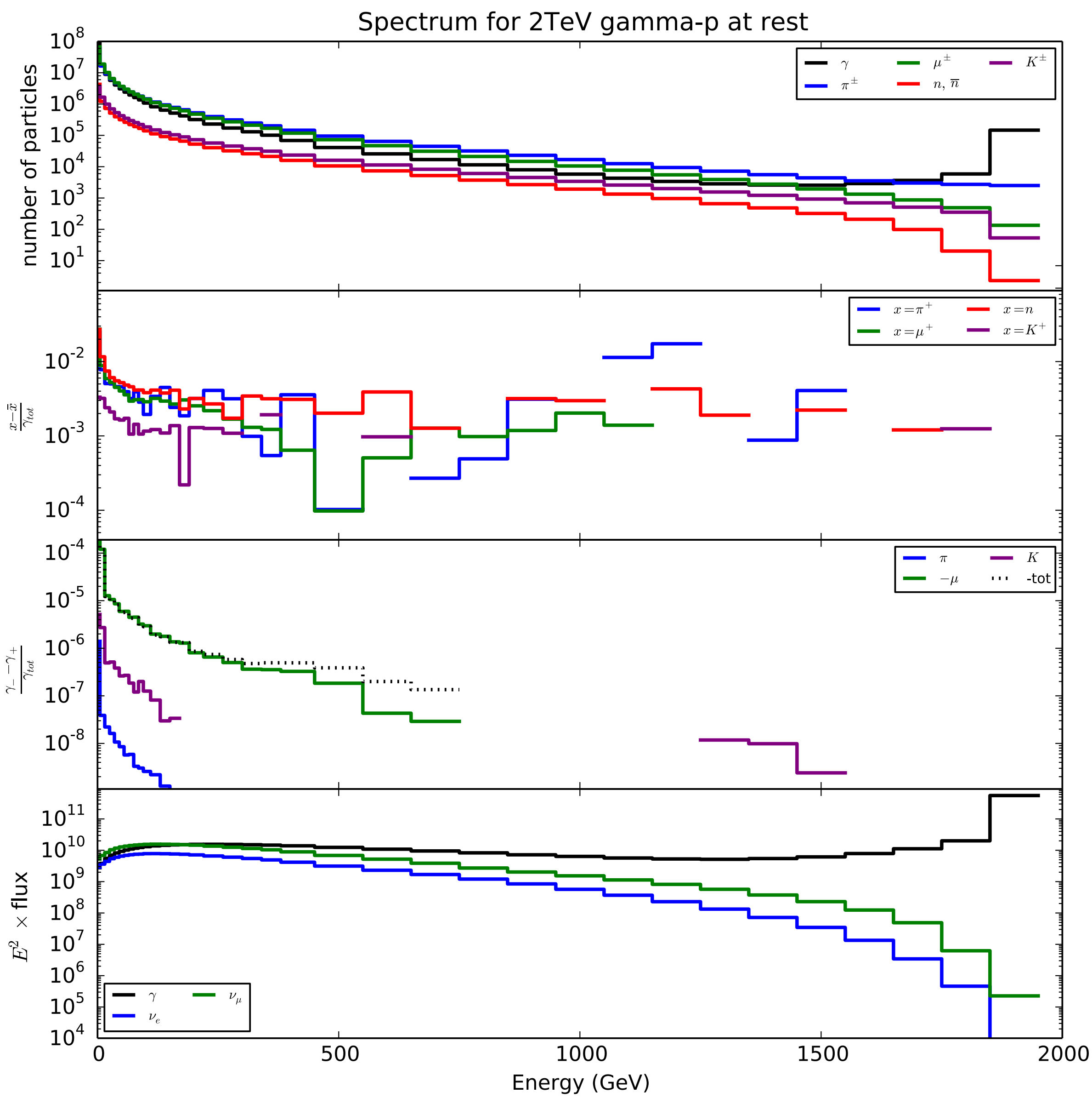

FIG. 10. Same as Fig. 5 for 2 TeV photons hitting protons at rest (number of events is 10^7). We have not included the effects of propagation which lead to attenuation and appearance of an energy cutoff.

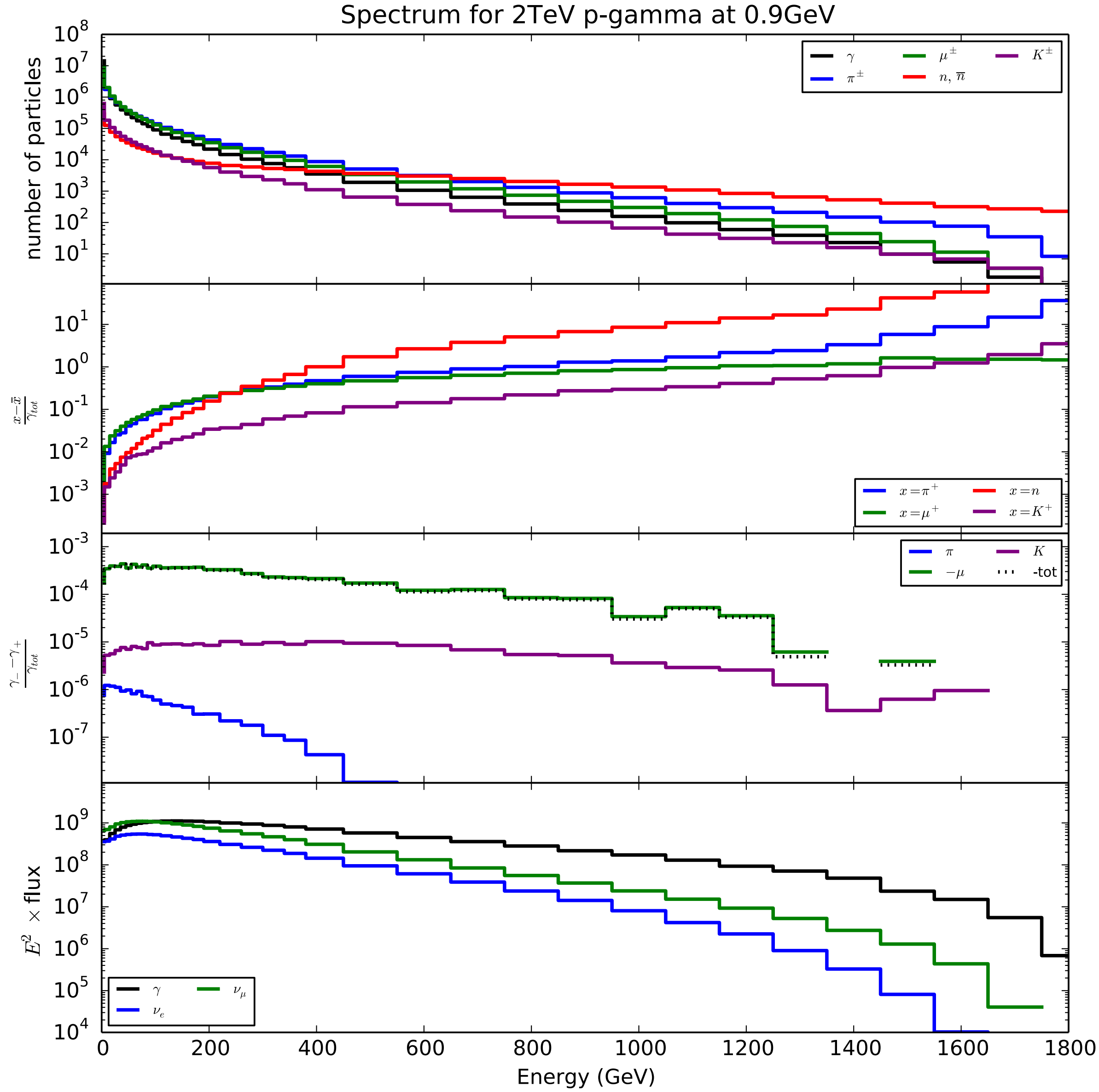

FIG. 11. Same as Fig. 5 for 2 TeV protons hitting low-energy photons (number of events is 10^6). We have not included the effects of propagation which lead to attenuation and appearance of an energy cutoff.

correspond to such a gamma hitting a proton from the interstellar medium. The asymmetry between particles and antiparticles, including the neutrinos, as well as the net photon circular polarisation, are a few orders of magnitude lower than for proton-proton collisions. This significant difference between γp and pp collisions is due to the charge asymmetry of the proton remaining at rest and not being boosted to high energy like in the pp collisions. Figure 11 displays the opposite case: a high-energy proton (with large charge momentum) hitting a low-energy photon. In this case, the polarization fraction is similar to the pp collisions. Although the total polarization fraction is Lorentz invariant, the distributions and cuts are done in the observer frame and are at the origin of the difference between those two cases.

IV. DISCUSSION

In the above sections, we have shown that hadronic processes in high-energy astrophysical environments can give rise to a non-negligible fraction of circularly polarized gamma rays. An observation of such a signal from a high-energy source would therefore help confirm the picture of a dominant hadronic component in AGN jets and tell us whether neutrino production is occurring in an optically thin environment. Other scenarios can benefit from precision measurements of circular polarization: if the majority of gamma rays are produced by proton synchrotron, as in [31], or if both hadrons and leptons contribute to the neutrino flux (e.g. [32]), then a simple ratio of gamma ray-to-neutrino fluxes become insufficient.

Depending on the measured value for the polarization, we could furthermore discriminate between two scenarios based on the fact that proton-proton collisions lead to a much stronger polarization signal than collisions of high-energy photons on stationary protons.

Furthermore, circular polarization has recently been proposed as a signal of new physics [8,9]. The polarization produced by electroweak processes as described here is part of the background to such searches. Our result shows that this background is relatively small and almost independent of energy. Both are good news for new physics searches.

A. Other sources of polarization

Some leptonic fraction in CR acceleration sites is inevitable: synchrotron emission has been inferred from the linear polarisation of ultraviolet emission of at least one Blazar. In an AGN jet, leptonic emission mechanisms at high energies fall into two flavors of inverse Compton scattering [33] which are as follows:

(1) Synchrotron self-Compton, wherein synchrotron emission is scattered to higher energies by a jet's relativistic electrons;
(2) External Compton (EC) scattering, either with the photons from the accretion disk, or with clouds external to the galaxy.

Compton scattering leads to some suppression of the polarization fraction, but this amounts only to a few percent at the high energies $E_\gamma \gg m_e$ considered here [34].

Synchrotron radiation leads to both linear and circular polarizations depending on the relative direction between the magnetic field and the observer and is present also for lower-energy photon. Therefore, circular polarization from synchrotron radiation and hadronic processes can be distinguished according to their degree of correlation with the magnetic field, which can be inferred from the Faraday rotation of radio emission.

EC can yield GeV and higher photons; however, in the absence of a polarized electron flux, it would not yield a polarized gamma-ray signal. If the jet magnetic field polarizes the high-energy electrons, any asymmetry between e^+ and e^- could plausibly lead to a polarized signal. Such an effect can be controlled by looking for a correlated neutrino signal, as we discussed in Sec. II C.

Birefringence of the intergalactic medium induced by strong magnetic fields (the Cotton-Mouton effect) can act as a source of circular polarization; however, this requires very strong magnetic fields ($\sim m_e^2/e$).

B. Future prospects

Measuring such a polarized gamma-ray flux is obviously an observational challenge. Circular gamma-ray polarization has been measured in the laboratory [35–37], so prospects for applying such techniques to astronomy are not unreasonable. We leave an exact characterization of the flux normalization and background contributions to future work, as this requires detailed modeling of specific CR acceleration sites and the inclusion of distance-dependent propagation effects.

There is an interesting opportunity to verify this work prior to observing individual sources of high-energy photons of cosmic origin. The atmosphere is also a target for high-energy protons and the pp collisions produce the same degree of photon polarization. It might be possible to detect this polarization in future experiments and verify some of the theoretical models that we have used. Calculations would need to be modified to account for heavier cosmic ray isotopes, as well as the finite muon lifetime. The latter would reduce, and above certain energies, flip the relative polarization of the signal.

V. SUMMARY

Many processes at the origin of cosmic rays, including hadronic processes such as proton-proton or proton-photon collisions, are expected to happen much more often that their CP-conjugate process due to the asymmetry between matter and antimatter in the observable Universe. The matter-antimatter asymmetry of the initial state results in an asymmetry between particle and antiparticle produced by the hadronic shower. This fact combined with the presence of parity violation in the SM implies that they generate an asymmetry in the two circular polarizations of the resulting photons. Here, we have computed the circular polarization fraction of the photons produced by the radiative decays following those two processes and showed that they are about 5×10^{-4} for both proton-proton collisions or collisions of energetic protons on low-energy photons. However, the polarization fraction drops by more than 1 order of magnitude if the photon is carrying most of the energy of the collision and the proton is at rest. Here, we have considered several extreme scenarios/processes to illustrate how the polarization fraction varies. While only some of them are expected to give the dominant contributions for many astrophysical sources, other processes such as high-energy photon collisions with protons at rest would only give a small contribution. This small contribution may increase if less extreme kinematics are chosen (lower-energy photon on low-energy proton, etc.) and their polarization fraction will be closer but still different from the $p-p$ case. Eventually, precise polarization measurements in the far future will pinpoint the various contributions. Therefore, our results provide a test of the dynamics of distant objects as the primary acceleration mechanism has never been directly tested. While polarized light can also be induced by other processes such as synchrotron radiation or Compton scattering, the processes that we have focused on also lead to a correlated neutrino flux which we have explicitly derived and is uncorrelated with the magnetic field of the source.

ACKNOWLEDGMENTS

We thank Christine Rasmussen and Peter Skands for their help with PYTHIA. We also thank Frank Krauss for useful discussions. The work of C. D. was supported by the Fund for Scientific Research F.N.R.S.through the F.6001.19 convention. J. S. is grateful for support from COFUND. A. C. V. is supported by the Arthur B. McDonald Canadian Astroparticle Physics Research Institute, the Canadian Foundation for Innovation and the Ontario Ministry of Economics Development, Job Creation and Trade (MEDJCT). Research at Perimeter Institute was supported by the Government of Canada through the Department of Innovation, Science, and Economic Development, and by the Province of Ontario through MEDJCT.

APPENDIX: MONTE CARLO BOOST TO LAB FRAME

1. Pion three-body decay

\We start with the three-body decay $\pi^\pm \to \mu^\pm \nu_\mu \gamma$. We are only interested in the photon, so the muon energy y can be integrated over. We first randomly select a photon energy in the pion's rest frame, with a probability $P(E_\gamma) \propto dN_\gamma/dE_\gamma = d\Gamma_\pi/(\Gamma_\pi dE_\gamma)$. Randomly selecting a value of $\cos\theta$ in the uniform interval $[-1, 1]$, and $\phi \in [0, 2\pi]$ fully specifies the photon's four-momentum vector,

$$k^\alpha \equiv (E_\gamma, E_\gamma \cos\phi \sin\theta, E_\gamma \sin\phi \sin\theta, E_\gamma \cos\theta). \quad \text{(A1)}$$

The isotropy of the photon emission allows us to choose a coordinate system such that the pion is traveling in the x^1 direction. Then the photon's four-momentum in the lab frame is

$$k^\alpha_{lab} = \Lambda^\alpha_\beta k^\beta. \quad \text{(A2)}$$

If we are looking at a single pion energy $E_\pi = \gamma m_\pi$, then Λ is trivial,

$$\Lambda = \begin{pmatrix} \gamma & -\beta\gamma & 0 & 0 \\ -\beta\gamma & \gamma & 0 & 0 \\ 0 & 0 & 1 & 0 \\ 0 & 0 & 0 & 1 \end{pmatrix}. \quad \text{(A3)}$$

However, if the pions are rather distributed with a spectrum of energies, we must select a boost from that distribution. In doing this, we also need to remember that the higher-energy pions will decay slower by a factor of $1/\gamma$, due to time dilation. This is completely equivalent to a suppression in the spectrum. Thus, we pick γ from a distribution

$$P(\gamma) \propto \frac{1}{\gamma}\frac{dN_\pi}{d\gamma}. \quad \text{(A4)}$$

Repeating this process produces the lab frame distribution of energies (k^0_{lab}) and momenta. Binning these energies is equivalent to integrating over an isotropic power law spectrum.

2. Two-step muon decay

The next scenario is the two-body decay $\pi^\pm \to \mu^\pm \nu_\mu$, followed by $\mu^\pm \to \gamma e^\pm \nu_e \nu_\mu$. Again, we proceed in "reverse" order, first boosting the final-state photon from the muon frame to the parent pion frame, then to the lab frame following some initial distribution of pions. As before, the initial photon distribution is isotropic in its parent frame (assuming we do not know the direction of the muon's spin), so Eq. (A1) can be used to generate the initial photon four-momentum, but this time using the muon decay spectrum.

The photon's four-vector in the pion frame is $k'^\alpha = \Lambda^\alpha_\beta k^\beta$, though this time the boost is simple, since the two-body pion decay produces monoenergetic muons, with $\gamma = (m_\pi/m_\mu + m_\mu/m_\pi)/2 = 1.0417$.

Now, we do not know which direction the muon was emitted in, with respect to the pion's direction of travel. This rotation must be done in the frame of the pion on k'^α. We can either randomly generate a rotation matrix, or simply replace the spatial components of k' with a randomly oriented vector with the same norm, using the prescription above for selecting random angles on a sphere. Schematically, we denote this new vector

$$k''^\alpha = R^\alpha_\beta \Lambda^\beta_\nu k'^\nu, \quad \text{(A5)}$$

remembering that $R^\alpha_0 = R^0_\beta = 0$.

The final step is to boost back to the lab frame, given a pion energy distribution. The rotation above has allowed us to specify the pion direction of travel. The distribution is as above, except that we also need to account for the time-dilated muon decay rate. Fortunately, the muon's rest frame is very close to the pion's (since $\gamma_\mu = 1.04 \sim 1$), so this is dominated by the differences between the lab frame and the pion frame. This just means that there are now two time dilation factors: one slowing down pion decay and one further slowing down muon decay,

$$P(\gamma) \propto \frac{1}{\gamma^2}\frac{dN_\pi}{d\gamma}. \quad \text{(A6)}$$

[1] L. A. Anchordoqui, Ultra-high-energy cosmic rays, Phys. Rep. **801**, 1 (2019).

[2] R. D. Blandford and A. Königl, Relativistic jets as compact radio sources, Astrophys. J. **232**, 34 (1979).

[3] H. Krawczynski, Tev blazars–observations and models, New Astron. Rev. **48**, 367 (2004).

[4] M. G. Aartsen *et al.* (IceCube Collaboration), Evidence for high-energy extraterrestrial neutrinos at the IceCube detector, Science **342**, 1242856 (2013).

[5] M. G. Aartsen *et al.* (IceCube Collaboration), First Observation of PeV-Energy Neutrinos with IceCube, Phys. Rev. Lett. **111**, 021103 (2013).

[6] R. Blandford, D. Meier, and A. Readhead, Relativistic jets in active galactic nuclei, Annu. Rev. Astron. Astrophys. **57**, 467 (2019).

[7] F. M. Rieger, E. de Ona-Wilhelmi, and F. A. Aharonian, TeV astronomy, arXiv:1302.5603.

[8] C. Boehm, C. Degrande, O. Mattelaer, and A. C. Vincent, Circular polarisation: A new probe of dark matter and neutrinos in the sky, J. Cosmol. Astropart. Phys. 05 (2017) 043.

[9] A. Elagin, J. Kumar, P. Sandick, and F. Teng, Prospects for detecting a net photon circular polarization produced by decaying dark matter, Phys. Rev. D **96**, 096008 (2017).

[10] F. W. Stecker, C. Done, M. H. Salamon, and P. Sommers, High-Energy Neutrinos from Active Galactic Nuclei, Phys. Rev. Lett. **66**, 2697 (1991).

[11] E. Gabrielli and L. Trentadue, Light mesons and muon radiative decays and photon polarization asymmetry, Nucl. Phys. **B792**, 48 (2008).

[12] C. Patrignani *et al.* (Particle Data Group), Review of particle physics, Chin. Phys. C **40**, 100001 (2016).

[13] J. Alvarez-Muniz and F. Halzen, Possible high-energy neutrinos from the cosmic accelerator RX J1713.7-3946, Astrophys. J. **576**, L33 (2002).

[14] T. K. Gaisser, R. Engel, and E. Resconi, *Cosmic Rays and Particle Physics* (Cambridge University Press, Cambridge, United Kingdom, 2016).

[15] F. Halzen, High-energy neutrino astrophysics, Nat. Phys. **13**, 232 (2017).

[16] T. Sjostrand, S. Mrenna, and P. Z. Skands, PYTHIA6.4 physics and manual, J. High Energy Phys. 05 (2006) 026.

[17] T. Sjostrand, S. Mrenna, and P. Z. Skands, A brief introduction to PYTHIA8.1, Comput. Phys. Commun. **178**, 852 (2008).

[18] T. Sjostrand, S. Ask, J. R. Christiansen, R. Corke, N. Desai, P. Ilten, S. Mrenna, S. Prestel, C. O. Rasmussen, and P. Z. Skands, An introduction to PYTHIA8.2, Comput. Phys. Commun. **191**, 159 (2015).

[19] J. Alwall, M. Herquet, F. Maltoni, O. Mattelaer, and T. Stelzer, MadGraph5: Going beyond, J. High Energy Phys. 06 (2011) 128.

[20] J. Alwall, R. Frederix, R. Frederix, S. Frixione, V. Hirschi, F. Maltoni, O. Mattelaer, H.-S. Shao, T. Stelzer, P. Torrielli, and M. Zaro, The automated computation of tree-level and next-to-leading order differential cross sections, and their matching to parton shower simulations, J. High Energy Phys. 07 (2014) 079.

[21] M. Aaboud *et al.* (ATLAS Collaboration), Measurement of the Inelastic Proton-Proton Cross Section at $\sqrt{s} = 13$ TeV with the ATLAS Detector at the LHC, Phys. Rev. Lett. **117**, 182002 (2016).

[22] P. Skands, S. Carrazza, and J. Rojo, Tuning PYTHIA8.1: The Monash 2013 tune, Eur. Phys. J. C **74**, 3024 (2014).

[23] A. Donnachie and P. V. Landshoff, Elastic scattering and diffraction dissociation, Nucl. Phys. **B244**, 322 (1984).

[24] A. Alloul, N. D. Christensen, C. Degrande, C. Duhr, and B. Fuks, FeynRules 2.0—A complete toolbox for tree-level phenomenology, Comput. Phys. Commun. **185**, 2250 (2014).

[25] C. Degrande, C. Duhr, B. Fuks, D. Grellscheid, O. Mattelaer, and T. Reiter, UFO—The universal FeynRules output, Comput. Phys. Commun. **183**, 1201 (2012).

[26] A. Castellina, Cosmic ray composition and energy spectrum above 1-TeV: Direct and EAS measurements, Nucl. Phys. B, Proc. Suppl. **97**, 35 (2001).

[27] A. M. Sirunyan *et al.* (CMS Collaboration), Measurement of charged pion, kaon, and proton production in proton-proton collisions at $\sqrt{s} = 13$ TeV, Phys. Rev. D **96**, 112003 (2017).

[28] S. Aid *et al.* (H1 Collaboration), Measurement of the total photon-proton cross-section and its decomposition at 200-GeV center-of-mass energy, Z. Phys. C **69**, 27 (1995).

[29] A. U. Abeysekara *et al.* (HAWC Collaboration), Measurement of the crab nebula at the highest energies with HAWC, Astrophys. J. **881**, 134 (2019).

[30] M. Amenomori *et al.*, First Detection of Photons with Energy Beyond 100 TeV from an Astrophysical Source, Phys. Rev. Lett. **123**, 051101 (2019).

[31] H. Zhang, K. Fang, H. Li, D. Giannios, M. Böttcher, and S. Buson, Probing the emission mechanism and magnetic field of neutrino blazars with multiwavelength polarization signatures, Astrophys. J. **876**, 109 (2019).

[32] A. Keivani, K. Murase *et al.*, A multimessenger picture of the flaring blazar TXS $0506+056$: Implications for high-energy neutrino emission and cosmic-ray acceleration, Astrophys. J. **864**, 84 (2018).

[33] G. Ghisellini and P. Madau, On the origin of the γ-ray emission in blazars, Mon. Not. R. Astron. Soc. **280**, 67 (1996).

[34] C. Boehm, A. Olivares-Del Campo, M. Ramirez-Quezada, and Y.-L. Zhou, Polarisation of high energy gamma-rays after scattering, J. Cosmol. Astropart. Phys. 12 (2019) 041.

[35] S. Tashenov, Circular polarimetry with gamma-ray tracking detectors, Nucl. Instrum. Methods Phys. Res., Sect. A **640**, 164 (2011).

[36] S. Tashenov, T. Bäck, R. Barday, B. Cederwall, J. Enders, A. Khaplanov, Yu. Fritzsche, A. Surzhykov, V. A. Yerokhin, and D. Jakubassa-Amundsen, Electron polarimetry with Bremsstrahlung, J. Phys. Conf. Ser. **488**, 012057 (2014).

[37] M. Goldhaber, L. Grodzins, and A. W. Sunyar, Helicity of neutrinos, Phys. Rev. **109**, 1015 (1958).